ACS APPLIED MATERIALS & INTERFACES

Research Article

www.acsami.org

Ionomer Based Blend as Water Vapor Barrier Material for Organic Device Encapsulation

Sindhu Seethamraju,[†] Praveen C. Ramamurthy,*[,†,‡] and Giridhar Madras[†]

[†]Centre for Nanoscience and Engineering, Indian Institute of Science, Bangalore, 560012, India

[‡]Department of Materials Engineering, Indian Institute of Science, Bangalore, 560012, India

Supporting Information

ABSTRACT: Blends of poly (ethylene-*co*-methacrylic acid) (PEMA) and poly (vinyl alcohol-*co*-ethylene) (EVOH) were studied for encapsulating Schottky structured organic devices. A calcium degradation test was used to determine water vapor transmission rates and to determine the moisture barrier performance of neat and blend films. Moisture barrier analysis for the neat and blend compositions was discussed concerning the interactions in the blend, diffusivity of water molecules through the unit cell systems, and the occupiable free volumes available in the unit cells using molecular dynamics simulations. The experimental results of water vapor permeation were correlated with diffusion behavior predicted from molecular dynamics simulations results. The effectiveness of the blend as a suitable barrier material in increasing the lifetime of an encapsulated Schottky structured organic device was determined.

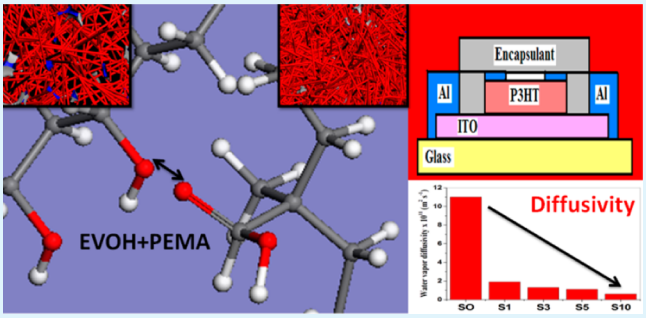

KEYWORDS: *encapsulant, polymer blends, calcium degradation test, water vapor diffusivity, molecular simulation*

1. INTRODUCTION

Moisture barrier materials have a wide range of domestic applications for construction and food packaging and also for sensitive applications like pharmaceutical and organic electronics packaging.[1−3] Development of high moisture barrier material, viable economically, is critical for all packaging applications. Recent progress in the field of organic electronics[4−6] has led to the increased flexible barrier material requirements toward moisture and oxygen for the encapsulation. The presence of moisture influences the active layer resulting in change of morphology and/or delamination of the interface of the active layer/electrode and increases the extent of oxidation. This causes the decrease in current density. Thus, the working lifetime of the device decreases in presence of moisture. Hence, an encapsulant with high moisture barrier property is required in order to protect the device from a humid environment and to increase the lifetime of the device.[7−10] It is estimated that, in order to protect the organic devices from environmental conditions, flexible moisture barrier materials with water vapor transmission rate (WVTR) < 10^{-6} g m^{-2} day^{-1} and oxygen transmission rate (OTR) < 10^{-5} cm^3 m^{-2} day^{-1} are required.[3,11]

Various organic and inorganic materials are being used in layered architecture to achieve the barrier requirement.[12,13] In organic electronics packaging, the use of inorganic oxide layers reduces the moisture ingression but the loss in mechanical flexibility and formation of dark spots reduces the device performance.[14−16] Moreover, the complexity of the deposition processes involving physical/chemical vapor depositions and in large area processing makes it an economically unreliable solution. Hence, polymer based materials such as polymer nanocomposites are being extensively investigated for achieving ultra low permeable properties.[17,18]

In situ curable epoxy composite with amine functionalized alumina,[19] functionalized mesoporous silica based silicone composites,[20] and zinc oxide based poly (vinyl alcohol) nanocomposite[21] materials have been previously investigated for the purpose of organic device encapsulation. Polymer blends are investigated to obtain materials with various improved synergistic properties.[22] The specific interactions like electrostatic, ionic, and hydrogen bonding determine the extent of compatibility between the blended polymers, which defines the resultant property at the required temperature.[23,24] Polymeric blends without interactions between the two polymers result in incompatible blends. However, it is necessary for the blend to have specific interactions to achieve better barrier property by blending two polymers.[25]

In this study, the blend of poly (ethylene-*co*-methacrylic acid) (PEMA) neutralized with zinc for UV stability and poly (vinyl alcohol-*co*-ethylene) (EVOH) was used for organic device encapsulation. In order to design the flexible encapsulant with high moisture barrier where the permeation mechanism is diffusion dominant, ethylene based, amorphous, self-healable ionomer, PEMA has been chosen as the base material for the

Received: March 1, 2013
Accepted: April 23, 2013
Published: April 23, 2013

blend in the present study. PEMA is a highly chemical resistant polymer with a wide range of processing temperatures. Moreover, it is possible to encapsulate the device directly by hot tack without using any epoxy glue/sealant for sealing at the edges.

Ionomers are defined as polymers whose bulk properties are governed by ionic interactions within the polymer.[26] PEMA belongs to the category of amphiphilic polymers where the ethylene backbone is hydrophobic in nature with the pendant groups like methacrylic acid being capable of interacting with water by forming hydrogen bonds and with alcohol by forming ester linkages. The acid groups form aggregates in the amorphous matrix surrounded by ethylene crystalline chains. As defined by Eisenberg,[27] aggregates consist of several ion pairs (dimers), and according to the EHM model,[28] the ion pair acts like anchors holding the attached polymer chains. It provides physical cross-linking in the polymer structure, thereby reducing the mobility. This synergy between the thermal and mechanical transitions is due to the presence of secondary interactions like hydrogen bonding. The presence of reversible cross-links in forming network polymer results in the self-healing property of the ionomer. Hence, ionomers of ethylene/methacrylic acid are extensively being researched for various applications requiring self-healing property.[29,30]

Poly (vinyl alcohol-*co*-ethylene) is a copolymer of poly ethylene and vinyl alcohol which is a high oxygen barrier polymer in low humid environments. It has been used for various food and pharmaceutical packaging in coextruded/layered structures.[31] The polar −OH group of EVOH interacts with the incoming moisture resulting in plasticization of the polymer chains, thereby increasing the free volume and oxygen permeability.[32] The blend of PEMA ionomer and EVOH copolymer helps in forming an interacting intercomplex polymer structure with reduced gas permeability.[33]

The gas permeation mechanism through polymers involves the solution-diffusion mechanism[34] which is dependent on the availability of free volume as well as the interactions between the penetrant and the matrix polymer. In rubbery polymers like EVOH, the permeation of a polar molecule is solubility dominant whereas it is diffusion dominant in glassy polymers like PEMA. The penetrant molecules first get adsorbed onto the polymer surface dissolving in the matrix and then are followed by diffusion through the matrix based on concentration/pressure gradient. Solubility in glassy polymers is negligible. Further, a highly interacting matrix-permeant system helps in decreasing the diffusivity of the permeant through the glassy polymers.[35] Therefore, the fundamental interactions between the polymer, environment, and the permeant determine the permeability behavior of a system.[36] Diffusion of small molecules through a system is dependent on the size, shape, connectivity of the system, free volume available, thermodynamic factors, physical interactions between the barrier material and penetrant, and environmental parameters, and thus, it is a complicated phenomenon. However, the key parameters would be the barrier-permeant system interactions under experimental conditions. Hence, molecular dynamics simulation studies at experimental conditions to determine the permeant diffusivity values help to understand the fundamental factors affecting diffusion.

2. EXPERIMENTAL METHODS

2.1. Materials. Poly (ethylene-*co*-methacrylic acid) zinc salt with 9 wt % methacrylic acid (PEMA) and poly (vinyl alcohol-*co*-ethylene) containing 38% ethylene (EVOH) were purchased from Sigma Aldrich Ltd. (St. Louis, MO). Poly (3-hexylthiophene) (P3HT) was obtained from Rieke Metals Inc. Tetrahydrofuran (THF), chlorobenzene, and carbontetrachloride (CCl_4) solvents of 99.9% purity were obtained from SD. Fine Chem., India Ltd.

2.2. Film Fabrication. PEMA and EVOH in pellet form were dried in vacuum for 2 days prior to blending in Haake internal mini screw extruder at 80 rpm and 210 °C for 10 min under nitrogen atmosphere. They were blended in wt % of (PEMA ionomer, EVOH copolymer) at approximately (100, 0), (99, 1), (97, 3), (95, 5), and (90, 10) and designated as S0, S1, S3, S5, and S10, respectively. The extruded blend was compression molded at 200 °C by applying a force of 600 N for 1 min to fabricate into films. Thus obtained films were found to be ∼130 ± 20 μm thickness. These films were used for further characterizations.

2.3. Material Characterization. All the blend films were characterized using a Thermo-Nicolet 6700 IR spectrometer in the range of 400 to 4000 cm^{-1} at 4 cm^{-1} resolution. UV−visible analysis was carried out using a Perkin-Elmer Lambda-35 spectrometer in the wavelength range of 230 to 1100 nm with 1 nm interval. Thermal properties of the blend films were determined using a Mettler Toledo (DSC 822^e) instrument at a heating rate of 5 °C min^{-1} under nitrogen atmosphere. Mechanical properties were determined from tensile analysis of 4 samples for each composition using a Mecmeisin Micro Universal Testing Machine, with 10 kN load cell at a rate of 25 mm min^{-1} following ASTM D882-12 standard. The cryogenically fractured films were imaged using scanning electron microscopy (SEM) by a Karl Zeiss ULTRA 55 field emission scanning electron microscope. The fractured surfaces were sputter coated with gold and then used for SEM imaging. A Kaleidoscope (India Ltd.) humidity chamber was used for maintaining a controlled humid environment for calcium degradation and accelerated device aging experiments.

A density gradient column constructed following ASTM D1505 standard was used to determine the density of the films. The column of 1 m was filled with THF (886 kg m^{-3}) and CCl_4 (1590 kg m^{-3}), with increasing density compositions from top to bottom of the column. The mixtures of THF/CCl_4 (v/v) 100/0, 80/20, 70/30, 60/40, 50/50, 40/60, 30/70, 25/75, 20/80, 10/90, 5/95, and 0/100 were slowly poured into the column from the sides of the column wall. Standard density glass beads (H & D Fitzgerald Ltd.,St. Asaph, UK) were dropped into the column, and the column was calibrated for density using these positions. The sample films were then dropped slowly into the column one after another and allowed to settle.

2.4. Calcium Degradation Test. A calcium degradation test was used to determine the water vapor transmission and to calculate the water vapor diffusivity values through the neat and blend films. Calcium (density = ∂) of 200 nm thickness was thermally evaporated onto a 2 cm × 2 cm ($l \times b$) clean glass slide at the center using a shadow mask. Aluminum was thermally deposited on either side of calcium to provide electrical contact for measuring the resistance of calcium, as shown in Figure S1, Supporting Information. The calcium on the glass slides was sealed with the sample films using curable epoxy (Lapox L12, Atul Industries, India Ltd.). Thermal deposition of calcium and aluminum as well as calcium sealing were carried out inside a Mbraun glovebox (ultra high pure nitrogen atmosphere, H_2O < 10 ppm, O_2 < 10 ppm) integrated with a thermal evaporator. Thus, the sealed calcium on the glass slide reacts when the water vapor permeates through the film after placing it in a controlled humid environment of RH = 95% (±3%) and at 35 °C (±0.2 °C). This results in the increase of resistance (R) which is measured as a function of time (t) using a programmable digital multimeter.

When calcium reacts with moisture, the thickness of calcium deposited on the glass slide decreases with time. Hence, the resistance measured increases, and this change in resistance is correlated to the change in thickness. The change in thickness gives the amount of calcium reacted. The change in resistance, over the calcium thickness variation from 200 to 100 nm, was used for further calculation as the resistivity of calcium (ρ) is independent of calcium film thickness above 100 nm.[37] As one molecule of calcium can react with two molecules of H_2O, the water vapor permeated through the sample film

from the calcium test is determined using eq 1 where molecular weight of water is M_{H2O} (18) and that for calcium is M_{Ca} (40).[38]

$$\mathrm{WVTR} = -2\frac{M_{H_2O}}{M_{Ca}}\,\partial\rho\left(\frac{l}{b}\right)\frac{\mathrm{d}\left(\frac{1}{R}\right)}{\mathrm{d}t} \quad (1)$$

In eq 1, all the terms, except R and t, are constant. Hence, the change in R with t for all the sealed calcium with different barrier films was used to determine the WVTR through them.

Another control experiment was carried out to verify the WVTR through the cured epoxy by sealing a similarly calcium deposited glass slide with a glass slide using the same epoxy. The value of WVTR through the epoxy sealing was found to be negligible.

2.5. Simulation Details. Materials studio 6.0 (MS), Accelrys Inc., was used for generating bulk structures of PEMA and EVOH and for simulation studies of the neat PEMA and PEMA-EVOH blend systems. COMPASS (condensed-phase optimized molecular potentials for atomistic simulation studies) forcefield[39,40] was used during all the simulations for determining the energetic interactions.

Polymer chains were built following Markov transition probability scheme of MS Build module. The molecular chains of PEMA of chain length 33 were constructed with 9 wt % of methacrylic acid and EVOH of chain length 32 were built with 62 mol % of vinyl alcohol with chirality inversion probability of 1.0 and flip probability of 0. The part of the polymer molecular chain with the functional repeat unit for both the built polymer chain units of PEMA and EVOH polymers is given in Figure S2, Supporting Information. Thus, built molecular chains of polymers were optimized for geometry and minimized for energy initially. Throughout the simulations, all of the energy minimization procedures were followed by using a cascade algorithm starting with the steepest descent, changing to conjugate-gradient as the energy derivative on the atom reduces to 1000 kcal mol^{-1}. This is followed by the quasi Newton−Raphson method when it is below 10 kcal mol^{-1} and ends when the convergence limit of 2.0×10^{-5} kcal mol^{-1} is achieved.

The Amorphous Cell module is used to build unit cell systems with PEMA/EVOH (in wt %), 100:0 (neat) and 90:10 (blend), at 308 K and reduced densities of 0.4 g cm^{-3} following the method of Theodoreou and Suter.[41,42] Four H_2O molecules were inserted into the constructed neat and blend unit cells at various free volume sites. The neat and blend unit cell structures were energy minimized. Then, the optimized neat and blend unit cells were relaxed by subjecting them to a series of short spanned anneal dynamics and stage wise equilibration procedure. The anneal dynamics consisted of 5 anneal cycles from 300 to 500 K with 5 heating ramps per cycle. The system was compressed from 0.0001 GPa (atmospheric pressure) to 100 GPa gradually in 5 steps using constant pressure ensemble (NPT) dynamics at pressures of 0.0001, 0.01, 1, 10, and 100 GPa. The compressed system was finally relaxed to experimental density in 5 steps. Each NPT step was followed by constant energy (NVE) anneal dynamics for energy minimization with 5000 steps for 0.5 ps. All the simulation runs were conducted using Nose ensemble control method[43,44] with Q-ratio of 0.01 for temperature control and Berendsen control method[45] with decay constant of 0.1 ps for the pressure control. A relatively small time step of dt = 1.00 fs was used during all the equilibration steps. The main aim is to generate neat and blend unit cells depicting systems at experimental conditions of 308 K and 1 bar. The final structure resulting from relaxing the unit cell is equilibrated using NPT molecular dynamics (MD) for 50 ps at 308 K. For obtaining the mean square displacement (MSD) of H_2O molecules in the neat and blend systems, the final relaxed and equilibrated neat and blend unit cell structures were subjected to NVE MD simulation for 50 ps with a time step of 1.0 fs.

During all the simulations, the cut off for nonbonded interactions was considered as 18.5 Å with spline width of 1 Å and buffer width of 0.5 Å. The Ewald electrostatic summation method[46,47] was used with an accuracy of 10^{-5} kcal mol^{-1} at 6 Å of repulsive cutoff distance and 0.5 Å of buffer width.

2.6. Accelerated Aging Experiments. Organic devices were fabricated using 1.25 wt % of P3HT in chlorobenzene. 150 μL of P3HT solution was spin coated onto ITO coated glass slides at 1000 rpm for 1 min and then annealed at 110 °C for 10 min. Aluminum electrodes were thermally evaporated using a shadow mask as shown in Figure S3, Supporting Information. These fabricated Schottky structured organic devices were sealed with the blend films using an epoxy. Current voltage (I−V) characteristics for all the non-encapsulated and encapsulated devices were measured using a Keithley source meter (Model 2420). For accelerated device aging studies, devices were placed in a humid environment of 95% RH at 35 °C.

3. RESULTS AND DISCUSSION

When PEMA is blended with EVOH, the ethylene chains of the two polymers are compatible, and the −OH groups of EVOH and −COOH groups of PEMA result in a highly interacting blend.[33] This helps in decreasing the free volume available for the penetrant to permeate through the layer. Furthermore, both the polymers used for blending are capable of forming hydrogen bonds with permeating H_2O molecules. This helps in providing a strongly interacting environment for water molecules.

3.1. Characterizations. From the density profile (as given in Table 1), a density of 912 kg m^{-3} was observed for the neat ionomer film. With increasing EVOH content in the blend, density gradually increased to 936 kg m^{-3} for S10.

Table 1. Density and Transition Temperature for the Neat and Blend Films

sample	order−disorder transition temperature (°C)	melting point (°C)		density (kg m^{-3})
		PEMA	EVOH	
S0	41.8	92.1		912
S1	42.2	92.6	172.3	917
S3	41.8	92.4	172.3	927
S5	42.3	93.6	173.7	933
S10	42.1	93.6	173.7	936

Fourier transform infrared (FTIR) spectra for the neat and blend films is as shown in Figure 1, the peak observed at 720

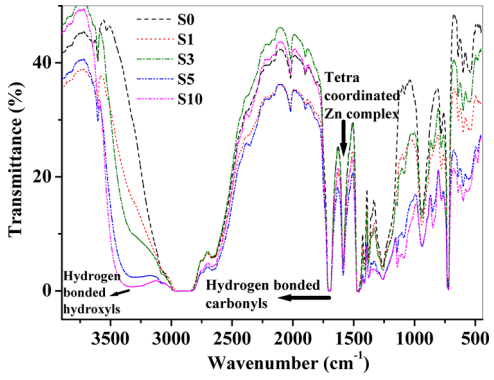

Figure 1. FTIR spectra for the neat and blend films.

cm^{-1} is caused by methylene rocking in the pendant backbone.[48] The peak at 1258 cm^{-1} is due to the C−O stretching vibrations of COOH groups in the hydrogen bonded dimers.[49] The peak intensity increased in the blend as compared to that in the neat ionomer because of the addition of EVOH. The bands found in the region 1400−1550 cm^{-1} are due to the (CO)O−C groups. Their intensity also increased

dx.doi.org/10.1021/am4007808 | ACS Appl. Mater. Interfaces 2013, 5, 4409−4416

from S0 to S10 films suggesting the interaction of −COOH ionomer with EVOH copolymer. This linkage would further help form an interacting ionomer blend. The single peak at 1587 cm^{-1} can be attributed to a symmetrizable single peak of carboxylate groups because of the presence of tetra coordinated Zn complexes in the blend films.[50,51] The peak at 1700 cm^{-1} is due to the hydrogen bonded carbonyl groups. The region from 3000 to 2900 cm^{-1} was an overlap of C−H stretching peaks in PEMA and EVOH. The broadened peak at ∼3330 cm^{-1} can be attributed to hydrogen bonded O−H groups, which was observed only in the blend films. Thus, the blend of ionomer and copolymer is compatible, because of the electrostatic interactions as well as hydrogen bonding, resulting in an interacting complex blend.

Differential scanning calorimetric (DSC) analysis for the neat and blend films for order−disorder transition (T_o) and melting temperatures (T_m) are tabulated in Table 1. The order−disorder transition temperatures[52,53] observed (Figure 2a) during first heating cycle for the neat film also appeared in the blend films. The ionic aggregates become disordered at T_o with the supply of thermal energy during the first heating. During the second heating cycle, these aggregates get suppressed and thus are not visible. T_o is associated with the reversible cross-link formation and self-healing capability of the ionomer. The addition of EVOH up to 10 wt % did not affect the ionomer in terms of ionic cluster formation. The melting temperatures (Figure 2b,c) at ∼92.1 °C (S0) and ∼172.1 °C (EVOH) for the neat, PEMA ionomer and EVOH copolymer slightly increased to 93.6 and 173.7 °C, respectively, for the blend film S10. This increase can be attributed to the increase in energy required to melt the polymer chains in the interacting complex blend system. The SEM images for the fractured film surfaces as given in Figure S4, Supporting Information, depict the increase in extent of crack formation with increasing EVOH content in the blend, suggesting the increased interfacial interactions due to the various possible interactions, in the interacting complex blend systems. The morphology of the neat ionomer consists of ionic aggregates of <1 nm.[54] The SEM images for the morphology of neat (S0) and blend (S5) films at different magnifications are given in Figure S5, Supporting Information. From Figure S5e,f, Supporting Information, it can be observed that both the neat and blend morphologies are similar with ionic aggregates distributed uniformly in liquid like fashion throughout. This is in coherence with the DSC analysis, that there is no change in ionic aggregate formation due to the addition of EVOH to PEMA.

It is observed from the stress/strain plots for all the blend films (Figure 3 and Table 2), that the tensile strength at break decreases with increasing EVOH content. The percentage elongation followed a decreasing trend from S0 to S10, i.e., with increasing EVOH content. This could be due to the decrease in chain flexibility arising due to the interactions between PEMA and EVOH chains. However, the percentage elongation was >70% for all the films. Hence, these blend films are suitable for flexible packaging applications.

The UV−visible spectroscopic analysis, given in Figure 4, suggests that the blend films are capable of absorbing UV radiation and thus can be used in organic electronics encapsulation applications to provide UV protection. The visible light transparency of the films increased with increasing EVOH content. Blend films exhibited greater than 50% transparency in the visible region (400−700 nm), and it gradually decreased in the UV region (230−400 nm).

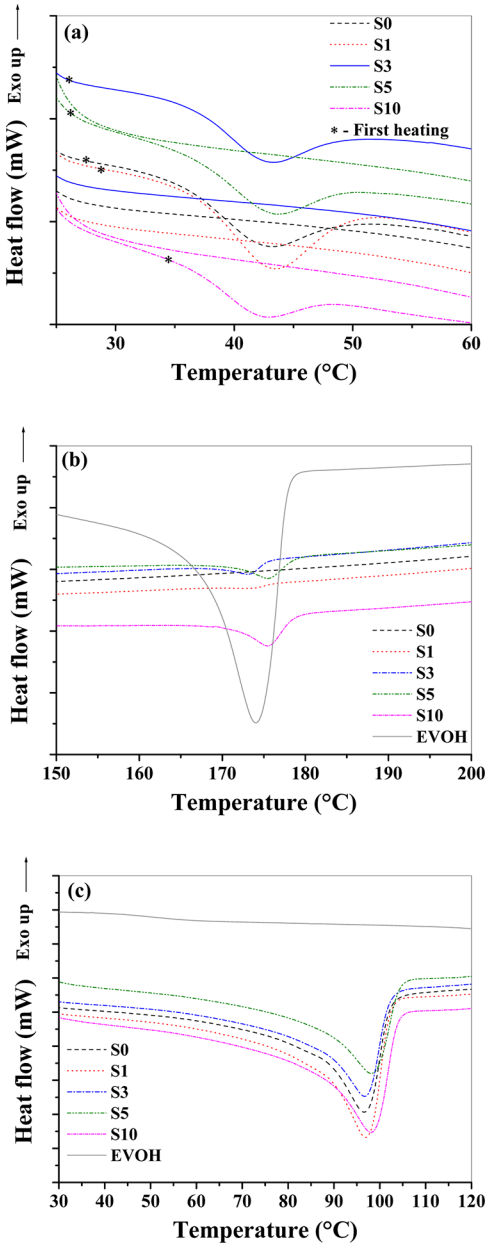

Figure 2. DSC thermograms for the neat and blend films (a) transition temperatures during first and second heating cycles, (b) EVOH melting peaks during second cycle, and (c) PEMA melting peaks during second cycle.

3.2. Calcium Degradation Test. From the calcium degradation test, the changes in the normalized conductance (R_o/R) of calcium with time for all the blend films at 95 ± 3% RH and T = 35 ± 0.2 °C are given in Figure 5a. The WVTR through the films was calculated for all the composite films and shown in Figure 5b. It can be observed that the WVTR value gradually decreased from S0 to S10 with increasing EVOH content. All the calcium tests were conducted under similar conditions. It can also be observed that, with increasing EVOH content, the time required for complete degradation of calcium also increased from 3000 to 10 000 s from S0 to S10 with increasing EVOH content. This can be attributed to the restricted moisture permeation through the blend system as compared to that through the neat film. The interactions in the blend decrease the free volume available for permeation. In

dx.doi.org/10.1021/am4007808 | ACS Appl. Mater. Interfaces 2013, 5, 4409−4416

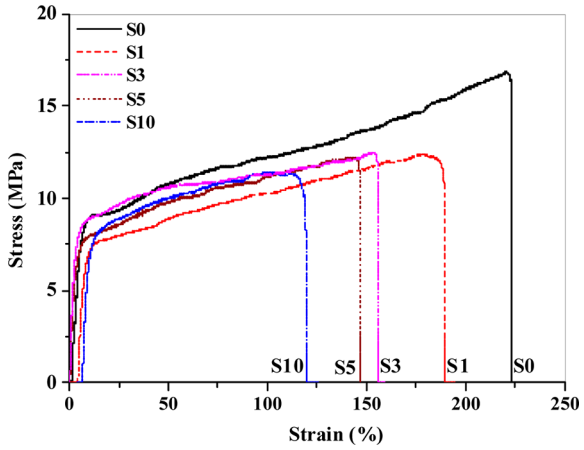

Figure 3. Tensile analysis for the neat and blend films.

Table 2. Tensile Properties of the Blend Films

sample	tensile strength at yield (MPa)	elongation at yield (%)	tensile strength at break (MPa)	elongation at break (%)
S0	9.0 ± 0.2	11 ± 1	16.7 ± 0.3	221 ± 5
S1	7.5 ± 0.3	11 ± 1	12.3 ± 0.1	184 ± 6
S3	7.5 ± 0.5	10 ± 2	12.1 ± 0.3	145 ± 5
S5	8.1 ± 0.2	10 ± 1	11.1 ± 0.2	116 ± 6
S10	8.2 ± 0.3	8 ± 1	10.7 ± 0.1	78 ± 8

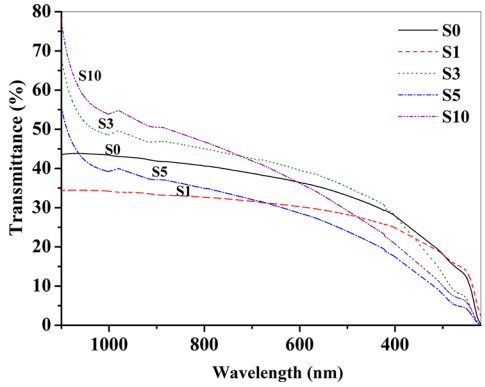

Figure 4. UV−visible absorption spectra for the neat and blend films.

addition, the permeant, being water vapor, must overcome the interactions from polar groups of EVOH and PEMA while penetrating through the film matrix. This increases the time required for the molecule to pass through the film. Hence, a gradual decrease in the determined diffusion coefficient for water vapor through the film was observed from S0 to S10, assuming the diffusion across a two-dimensional membrane, as calculated following a previously discussed method.[21] The relative decrease in WVTR by two orders and diffusivity by one order (Table 3) for S0 to S10, from the calcium degradation test, suggests the improvement in the barrier property of the blend system.

3.3. Simulation Results. The equilibrated and relaxed unit cells at experimental conditions for the neat and blend systems, after being subjected to NVE molecular dynamics simulations, resulted in 51 frames in 50 ps, which were used for calculating the MSD of the H_2O molecules through the system. The plots for averaged MSD of the four molecules of H_2O through the neat and blend unit cells are given in Figure 6a,b. The slope to calculate the diffusion coefficient is estimated from the linear

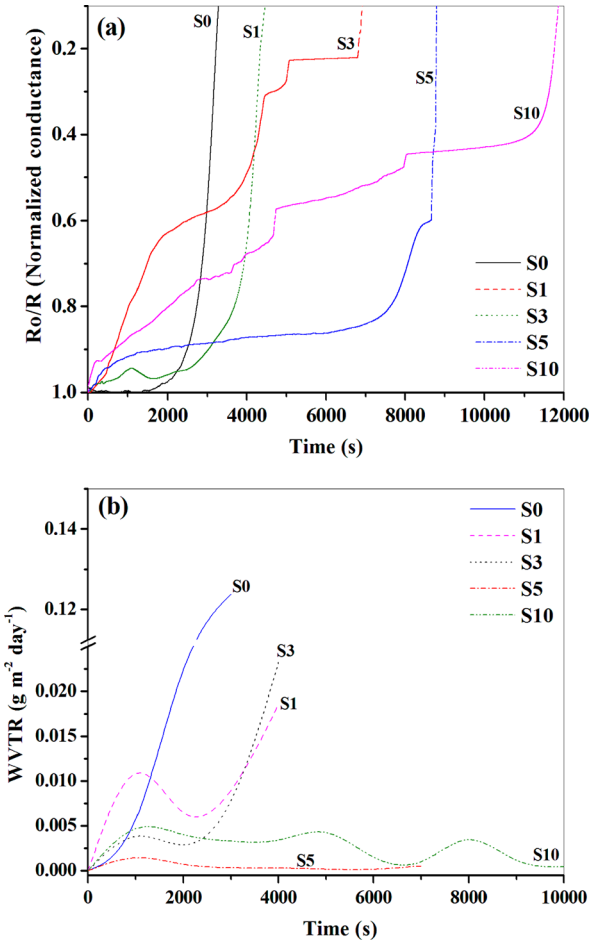

Figure 5. Water vapor permeation behavior through the blend and neat films from the calcium degradation test. (a) Decreasing conductivity of calcium and (b) WVTR comparison.

Table 3. Water Vapor Transmission Rate and Diffusivity Values Determined from a Calcium Degradation Test

	WVTR (g m^{-2} day^{-1})				
time (s)	S 0	S 1	S 3	S 5	S 10
0−1000	0.00230	0.0152	0.0053	0.0029	0.0061
1000−2000	0.09302	0.0040	0.0016	0.0050	0.0037
2000−3000	0.12380	0.0078	0.0055	0.0003	0.0033
3000−4000		0.0186	0.0232	0.0003	0.0029
4000−7000				0.0004	0.0030
7000−10000					0.0004
diffusion coefficient 10^{11} (m^2 s^{-1})	11	1.9	1.3	1.1	0.61

part of the MSD plot which corresponds to the Einstein diffusion limit. The calculated diffusivity value from simulation, for H_2O through the neat system, was 1.2×10^{-11} m^2 s^{-1} and through the blend system was 0.3×10^{-11} m^2 s^{-1}. The value of the diffusivity decreased in the blend system as compared to the neat system by a factor of 4. Furthermore, the value of the diffusivity calculated for the blend system (0.3×10^{-11} m^2 s^{-1}) from molecular simulations was found to be of the same order as that determined for S10 film (0.6×10^{-11} m^2 s^{-1}), from the calcium degradation test. The diffusivities do not match exactly with the experimental values because of the difference in the scales of calculations used for simulation (molecular level diffusion for a few ps) and for the calcium degradation test

dx.doi.org/10.1021/am4007808 | ACS Appl. Mater. Interfaces 2013, 5, 4409−4416

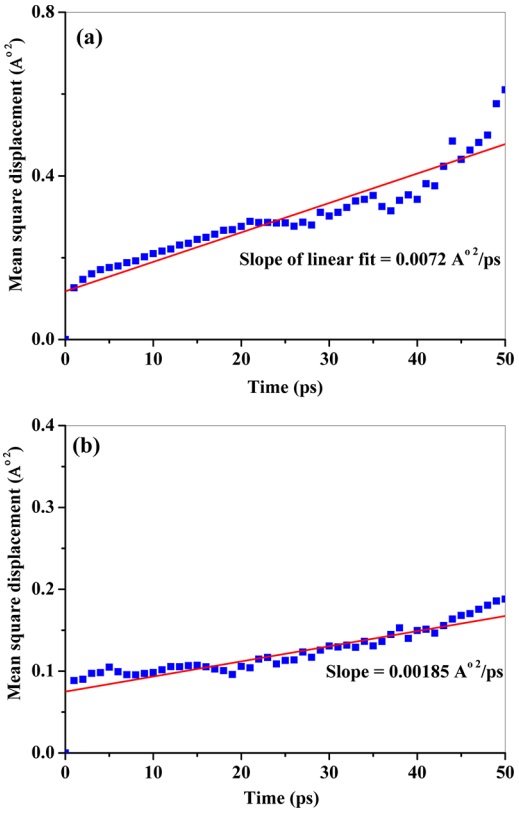

Figure 6. Mean square displacement of the four water molecules during 50 ps of NVE MD simulations at 35 °C and 1 bar in (a) neat and (b) blend unit cell systems. (Experimental data points are denoted by points, and the linear fit is the straight line.)

(diffusion through the bulk film of 130 μm thick in a few seconds).

The occupiable free volumes determined with various solvent probe radii for both the neat and blend, equilibrated and relaxed unit cells, at time t = 50 ps of the MD simulation are given in Table 4. The probe radii from 0.5 to 0.9 Å were used as the range which is much less than the mean molecular radius of H_2O molecule (1.3 Å)[55] as well as O−H bond distance of 0.99 Å.[56] The occupiable volume with respect to the occupied volume is relatively less in the blend system when compared to that in the neat system at all probe radii. The free volume available for the H_2O molecules to diffuse through the blend system is less than that in the neat system. Hence, the reduction in space available for H_2O diffusion decreased the displacement of the molecule in the blend system in agreement with the lower diffusivity values observed from both the simulation and experimental studies. With an increase in the probe radius, the free volume available for permeation was reduced in both the systems. The representative snapshots of the occupiable volumes in van der Waals representation are given in Figure 7a,b.

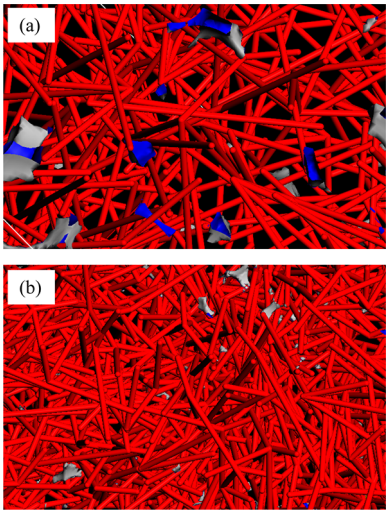

Figure 7. van der Waals representation of the occupiable free volumes (blue colored) for the (a) neat and (b) blend unit cells at 0.7 Å of solvent probe radius.

The channel formation for the molecule to permeate is dependent on the mobility of the polymer chains in the system. The mobility of chains in the neat and blend systems were compared by calculating the autocorrelation functions for the torsion angle of the C−C(O)−O group of PEMA chains over the 50 ps of MD simulations. The autocorrelation functions can be used to compare the limiting time for losing memory about the initial configuration. The local relaxation dynamics of the PEMA chain was calculated by determining the decay time for the autocorrelation function of the torsion angle for the C−C(O)−O group. From Figure 8, it is observed that C−C(O)−O groups of PEMA decorrelate the memory of their initial conformation more quickly for the neat system when compared with the blend system. It implies that the PEMA chains in the neat system are more dynamic compared to the blend system. The interactions between the C−C(O)−O of PEMA and OH groups of EVOH decreased the chain mobility. The decreased chain mobility in the blend system helps to decrease the extent of channel formation for H_2O diffusion, supporting the observed decrease in value of diffusivity. The effect of decreased chain mobility can also be observed from degradation in tensile property with increasing EVOH content in the blend.

3.4. Accelerated Weathering Studies. On the basis of current−voltage (I−V) characteristics (see Supporting Information, Figure S6), all the devices behaved as Schottky barrier devices. I−V characteristics for all the Schottky structured devices were measured initially (at time t = 0) and after accelerated aging (95% RH at 35 °C). After time, t of

Table 4. Occupiable Volumes for Different Probe Radii Determined from Molecular Dynamics Simulations

	occupied volume (Å^3)		occupiable free volume (Å^3)		solvent surface area (Å^2)	
probe radius (Å)	neat	blend	neat	blend	neat	blend
0.6	44817.16	48745.07	152.51	144.97	1483.97	1455.05
0.7	44941.12	48865.91	28.55	24.13	298.21	256.15
0.8	44966.16	48887.62	3.58	2.42	38.13	25.4
0.9	44969.41	48889.85	0.27	0.19	2.92	2.14

dx.doi.org/10.1021/am4007808 | ACS Appl. Mater. Interfaces 2013, 5, 4409−4416

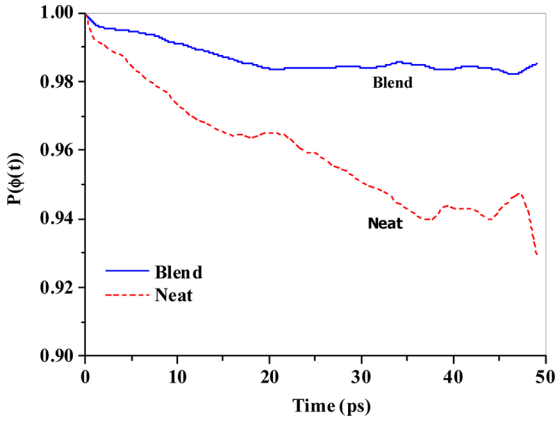

Figure 8. Comparison for decay times of the autocorrelation function for the C−C(O)−O torsion angle distributions in the neat and blend systems.

aging, the percentage reduction in current density with respect to the initial current density for all the devices was calculated from *I*−*V* characteristics (within 0 to 1 V range). The percentage loss in device performance was calculated for using the following equations:

$$\%\ \text{change in current density} = \frac{\text{initial current density (at V)} - \text{current density at time } t \text{ (at V)}}{\text{initial current density (at V)}} \times 100$$

$$\%\ \text{loss in device perf ormance} = \text{average of \% change in current density over 0−1 V}$$

The loss in device performance with time was plotted as shown in Figure 9. It is observed that, after 15 min of

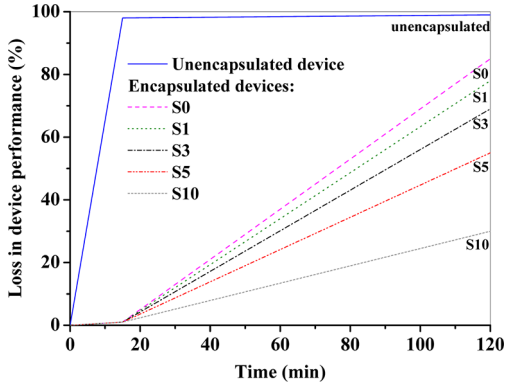

Figure 9. Encapsulated device performances in comparison to nonencapsulated devices determined from the loss in current over time.

accelerated aging, there is ∼98% loss in current density for the nonencapsulated device but the devices encapsulated with blend films lost by <3%. The encapsulated devices were stable for more than 60 min, retaining >50% of their initial performance. Furthermore, the device encapsulated with S10 film lost by only ∼30% of its initial performance, even after 120 min under accelerated conditions while the neat S0 film lost ∼80% of the performance. This is due to the decreased moisture diffusivity and the increased barrier property of the complex interacting blend used for encapsulation. From the device performance, calcium degradation test, and simulation results, the blend of PEMA and EVOH can be considered as a high moisture barrier material. This indicates that the blend can be used for high moisture barrier applications like organic device encapsulation.

The barrier layer increases the lifetime of the device by not allowing moisture to permeate through the film and reach the device. These blend films can further be improved for barrier property by addition of a third component capable of interacting with both the copolymers, by decreasing the chain mobility and free volume availability, or by increasing the diffusion pathway to the penetrant.

4. CONCLUSIONS

PEMA is an amorphous, self-healing ionomer, with diffusion dominant regime for permeation. A highly interacting complex blend was fabricated by addition of EVOH to ionomer which consequently improved the moisture barrier property of the blend. To retain the basic PEMA properties as discussed previously, EVOH content was restricted only up to 10 wt %. The blend resulted in electrostatic and hydrogen bond interactions between the two polymers, reducing the chain mobility and the free volume available for permeant diffusion affecting the tensile and barrier properties. The WVTRs calculated from the calcium degradation test decreased by two orders for the highest content of EVOH (10 wt %) in the blend. It further suggested that there is an increasing barrier property for the blend with an increase in EVOH content. The occupiable free volume determined from MD simulations was found to be relatively less for the blend as compared to the neat system. In addition, the values of diffusivity calculated from the simulations as well as from the calcium degradation test indicate an there is an improved barrier property with the addition of EVOH to PEMA. The accelerated weathering studies for the nonencapsulated and encapsulated organic devices proved the blend to be efficient by increasing the device lifetime to 120 min from 10 min by restoring more than 30% of the initial device performance. Therefore, blends of PEMA and EVOH can be used for high moisture barrier applications. Further improvement in the barrier and mechanical properties can be achieved with the addition of nanofillers to the blend.

■ ASSOCIATED CONTENT

Supporting Information

Schematic for calcium degradation test setup (Figure S1), part of the molecular chains of (a) EVOH and (b) PEMA with their repeat units (Figure S2), schematic for Schottky structured device encapsulation (Figure S3), SEM image for fractured surface of the films (a) S0, (b) S5, and (c) S10 compositions (Figure S4), SEM image for surface of the neat and blend films at different magnifications (a) S0 at 500 μm, (b) S5 at 500 μm, (c) S0 at 1 μm, (d) S5 at 1 μm, (e) S0 at 200 nm, and (f) S5 at 200 nm (Figure S5), and *I*−*V* characteristics for S10 encapsulated P3HT based Schottky device before and after accelerated aging (Figure S6). This information is available free of charge via the Internet at http://pubs.acs.org/.

■ AUTHOR INFORMATION

Corresponding Author

*Phone: 91-80-22932627. E-mail: onegroupb203@gmail.com.

Notes

The authors declare no competing financial interest.

■ ACKNOWLEDGMENTS

Authors gratefully acknowledge the financial support from DST No SR/S3/ME/022/2010-(G) and by the Ministry of Communication and Information Technology under a grant for the Centre of Excellence in Nanoelectronics, Phase II. Authors gratefully acknowledge Dr. Suryasarathi Bose of Materials Engineering Department, Indian Institute of Science, Bangalore, for providing the injection blending facility.

■ REFERENCES

(1) Feldman, D. *J. Polym. Environ.* **2001**, *9*, 49−55.
(2) Choi, M. C.; Kim, Y.; Ha, C. S. *Prog. Polym. Sci.* **2008**, *33*, 581−630.
(3) Moro, L.; Visser, R. J. In *Organic Photovoltaics*; Brabec, C., Dyakonov, V., Scherf, U., Eds.; Wiley-VCH Verlag GmbH & Co. KGaA: Weinheim, 2009; p 491.
(4) Steve, W. S.; Teresa, L. C.; David, E. B.; Biwu, M. *ACS Appl. Mater. Interfaces* **2012**, *4*, 2534−2540.
(5) Kelly, T. W.; Paul, F. B.; Chris, G.; David, E. E.; Dawn, M.; Michael, A. H.; Dennis, E. V.; Steven, D. T. *Chem. Mater.* **2004**, *16*, 4413−4422.
(6) Ramamurthy, P. C.; Harrell, W. R.; Gregory, R. V.; Sadanadan, B.; Rao, A. M. *Synth. Met.* **2003**, *137*, 1497−1498.
(7) Grossiord, N.; Kroon, J. M.; Ronn, A.; Paul, W. M. B. *Org. Electron.* **2012**, *13*, 432−456.
(8) Hong, Y. B.; Qun, S. L.; Cheng, G.; Chang, M. L. *Sol. Energy Mater. Sol. Cells* **2010**, *94*, 846−849.
(9) Kion, N.; Suren, G. A.; Frederik, K. C. *Appl. Mater. Interfaces* **2009**, *1*, 102−112.
(10) Mikkel, J.; Kion, N.; Frederik, K. C. *Sol. Energy Mater. Sol. Cells* **2008**, *92*, 686−714.
(11) Dennler, G.; Lungenschmied, C.; Neugebauer, H.; Sariciftci, N. S.; Labouret, A. *J. Mater. Res.* **2005**, *20*, 3224−3233.
(12) Wu, Z.; Wang, L.; Chun, C.; Qiu, Y. *J. Phys. D: Appl. Phys.* **2005**, *38*, 981−984.
(13) Dennler, G.; Lungenschmied, C.; Neugebauer, H.; Sariciftci, N. S.; Latreche, M.; Czeremuszkin, G.; Wertheimer, M. R. *Thin Solid Films* **2006**, *512*, 349−353.
(14) Roberts, A. P.; Henry, B. M.; Sutton, A. P.; Grovenor, C. R. M.; Briggs, G. A. D.; Miyamoto, T.; Kano, M.; Tsukahara, Y.; Yanaka, M. *J. Membr. Sci.* **2002**, *208*, 75−88.
(15) Chatham, H. *Surf. Coat. Technol.* **1996**, *78*, 1−9.
(16) da Silva, A. S.; Czeremuszkin, G.; Latreche, M.; Dennler, G.; Wertheimer, M. *Surf. Coat. Technol.* **1999**, *116*, 1204−1210.
(17) Chen, C. M.; Chung, M. H.; Hsieh, T. E.; Liu, M. O.; Lin, J. L.; Chu, W. P.; Tang, R. M.; Tsai, Y. S.; Juang, F. S. *Compos. Sci. Technol.* **2008**, *68*, 3041−3046.
(18) Kim, G. H.; Oh, J.; Yang, Y. S.; Do, L. M.; Suh, K. S. *Polymer* **2004**, *45*, 1879−1883.
(19) Gupta, S.; Ramamurthy, P. C.; Madras, G. *Polym. Chem.* **2011**, *2*, 221−228.
(20) Gupta, S.; Ramamurthy, P. C.; Madras, G. *Polym. Chem.* **2011**, *2*, 2643−2650.
(21) Gupta, S.; Sindhu, S.; Varman, K. A.; Ramamurthy, P. C.; Madras, G. *RSC Adv.* **2012**, *2*, 11536−11543.
(22) Brown, S. B. In *Polymer blends handbook*, 2nd ed.; Utracki, L. A., Ed.; Kluwer Academic Publishers: Netherlands, 2003, Vol. *1*; p 339.
(23) Kim, J. R.; Jamieson, A. M.; Hudson, S. D.; Manas-Zloczower, I.; Ishida, H. *Macromolecules* **1998**, *31*, 5383−5387.
(24) Chie, S.; Tetsuo, K. *Macromolecules* **1999**, *32*, 1949−1955.
(25) Painter, P. C.; Coleman, M. M. In *Polymer Blends*; Paul, D. R., Bucknall, C. B., Eds.; John Wiley & Sons, Inc.: New York, 2000; Vol. *1*, p 93.
(26) Eisenberg, A.; Rinaudo, M. *Polym. Bull.* **1990**, *24*, 671.
(27) Eisenberg, A. *Macromolecules* **1970**, *3*, 147−154.
(28) Eisenberg, A.; Hird, B.; Moore, R. B. *Macromolecules* **1990**, *23*, 4098−4107.
(29) White, S. R.; Sottos, N. R.; Geubelle, P. H.; Moore, J. S.; Kessler, M. R.; Sriram, S. R.; Brown, E. N.; Viswanathan, S. *Nature* **2001**, *409*, 794−797.
(30) Yang, F.; Pitchumani, R. *Macromolecules* **2002**, *35*, 3213−3224.
(31) Coleman, M. M.; Yang, X.; Zhang, H.; Painter, P. C. *J. Macromol. Sci., Phys.* **1993**, *32*, 295−326.
(32) Zhang, Z.; Britt, I. J.; Tung, M. A. *J. Appl. Polym. Sci.* **2001**, *82*, 1866−1872.
(33) Shelat, K. J.; Dutta, K. N; Choudhury, N. R. *Langmuir* **2008**, *24*, 5464−5473.
(34) Graham, T. *Philos. Mag.* **1866**, *32*, 401−420.
(35) Freeman, B. D.; Pinnau, I. *ACS Symposium Series*; American Chemical Society: Washington, DC, 1999; Vol. *733*, pp 1−27.
(36) Lodge, T. P. *J. Phys. Chem.* **1996**, *100*, 13275−13292.
(37) Renucci, P.; Gaudart, L.; Petrakian, J. P.; Roux, D. *Phys. Rev. B: Condens. Matter* **1982**, *26*, 5416−5425.
(38) Paetzold, R.; Winnacker, A.; Henseler, D.; Cesari, V.; Heuser, K. *Rev. Sci. Instrum.* **2003**, *74*, 5147−5150.
(39) Rigby, D.; Sun, H.; Eichinger, B. E. *Polym. Int.* **1998**, *44*, 311−330.
(40) Sun, H. *J. Phys. Chem. B* **1998**, *102*, 7338−7364.
(41) Theodorou, D. N.; Suter, U. W. *Macromolecules* **1985**, *18*, 1467−1478.
(42) Theodorou, D. N.; Suter, U. W. *Macromolecules* **1986**, *19*, 139−154.
(43) Nose, S. *J. Chem. Phys.* **1984**, *81*, 511−519.
(44) Nose, S. *Prog. Theor. Phys. Suppl.* **1991**, *103*, 1−46.
(45) Berendsen, H. J. C.; Postma, J. P. M.; van Gunsteren, W. F.; DiNiola, A.; Haak, J. R. *J. Chem. Phys.* **1984**, *81*, 3684−3690.
(46) Tosi, M. P. *Solid State Phys.* **1964**, *16*, 107−113.
(47) Ewald, P. P. *Ann. Phys.* **1921**, *64*, 253−287.
(48) Painter, P. C.; Brozoski, B. A; Coleman, M. M. *J. Polym. Sci., Part B: Polym. Phys.* **1982**, *20*, 1069−1071.
(49) Kutsumizu, S.; Hara, H.; Tachino, H.; Shimabayashi, K.; Yano, S. *Macromolecules* **1999**, *32*, 6340−6347.
(50) Han, K.; Williams, H. L. *J. Appl. Polym. Sci.* **1991**, *42*, 1845−1859.
(51) Coleman, M. M.; Lee, J. Y.; Painter, P. C. *Macromolecules* **1990**, *23*, 2339−2345.
(52) Tadano, K.; Hirasawa, E.; Yamamoto, H.; Yano, S. *Macromolecules* **1989**, *22*, 226−233.
(53) Kutsumizu, S.; Tadano, K.; Matsuda, Y.; Goto, M.; Tachino, H.; Hara, H.; Hirasawa, E.; Tagawa, H.; Muroga, Y.; Yano, S. *Macromolecules* **2000**, *33*, 9044−9053.
(54) Seitz, M. E.; Chan, C. D.; Opper, K. L.; Baughman, T. W.; Wagener, K. B.; Winey, K. I. *J. Am. Chem. Soc.* **2010**, *132*, 8165−8174.
(55) Carl, W. K.; Donald, R. W. *J. Chem. Phys.* **1972**, *56*, 4419−4421.
(56) Zeidler, A.; Salmon, P. S.; Fischer, H. E.; Neuefeind, J. C.; Simonson, J. M.; Markland, T. E. *J. Phys.: Condens. Matter* **2012**, *24*, 284126−284138.